An unusually powerful mode of low-frequency sound interference due to defective hair bundles of the auditory outer hair cells

Kazusaku Kamiya[a,b,c,d,1], Vincent Michel[a,b,c,1], Fabrice Giraudet[e], Brigitte Riederer[f], Isabelle Foucher[a,b,c], Samantha Papal[a,b,c], Isabelle Perfettini[a,b,c], Sébastien Le Gal[a,b,c], Elisabeth Verpy[a,b,c], Weiliang Xia[f], Ursula Seidler[f], Maria-Magdalena Georgescu[g], Paul Avan[e,2,3], Aziz El-Amraoui[a,b,c,2,3], and Christine Petit[a,b,c,h,2,3]

[a]Institut Pasteur, Génétique et Physiologie de l'Audition, 75015 Paris, France; [b]Institut National de la Santé et de la Recherche Médicale, Unité Mixte de Recherche, UMR-S 1120 Paris, France; [c]Sorbonne Universités, UPMC Univ Paris 06, Complexité Du Vivant, 75252 Paris Cedex 05, France; [d]Department of Otorhinolaryngology, Juntendo University Faculty of Medicine, Juntendo University, Tokyo 1138421, Japan; [e]Laboratoire de Biophysique Sensorielle, Faculté de Médecine, and Biophysique Médicale, Centre Jean Perrin, Université d'Auvergne, 63000 Clermont-Ferrand, France; [f]Department of Gastroenterology, Hepatology, and Endocrinology, Hannover Medical School, 30625 Hannover, Germany; [g]Department of Neuro-Oncology, The University of Texas MD Anderson Cancer Center, Houston, TX 77030; and [h]Collège de France, 75005 Paris, France

Edited* by A. J. Hudspeth, Howard Hughes Medical Institute, New York, NY, and approved May 8, 2014 (received for review March 25, 2014)

A detrimental perceptive consequence of damaged auditory sensory hair cells consists in a pronounced masking effect exerted by low-frequency sounds, thought to occur when auditory threshold elevation substantially exceeds 40 dB. Here, we identified the submembrane scaffold protein Nherf1 as a hair-bundle component of the differentiating outer hair cells (OHCs). *Nherf1*$^{-/-}$ mice displayed OHC hair-bundle shape anomalies in the mid and basal cochlea, normally tuned to mid- and high-frequency tones, and mild (22–35 dB) hearing-threshold elevations restricted to midhigh sound frequencies. This mild decrease in hearing sensitivity was, however, discordant with almost nonresponding OHCs at the cochlear base as assessed by distortion-product otoacoustic emissions and cochlear microphonic potentials. Moreover, unlike wild-type mice, responses of *Nherf1*$^{-/-}$ mice to high-frequency (20–40 kHz) test tones were not masked by tones of neighboring frequencies. Instead, efficient maskers were characterized by their frequencies up to two octaves below the probe-tone frequency, unusually low intensities up to 25 dB below probe-tone level, and growth-of-masker slope (2.2 dB/dB) reflecting their compressive amplification. Together, these properties do not fit the current acknowledged features of a hypersensitivity of the basal cochlea to lower frequencies, but rather suggest a previously unidentified mechanism. Low-frequency maskers, we propose, may interact within the unaffected cochlear apical region with midhigh frequency sounds propagated there via a mode possibly using the persistent contact of misshaped OHC hair bundles with the tectorial membrane. Our findings thus reveal a source of misleading interpretations of hearing thresholds and of hypervulnerability to low-frequency sound interference.

off-frequency detection | Usher syndrome | hearing impairment | Nherf2 | tail hypersensitivity

Mammalian hearing displays remarkable sensitivity, fine temporal acuity, and exquisite frequency selectivity, which contribute to auditory scene analysis and speech intelligibility. The first steps of sound processing, i.e., sound wave detection and neuronal encoding in the cochlea, are performed by two populations of hair cells, the inner hair cells (IHCs) and the outer hair cells (OHCs). These cells are sandwiched between the underlying basilar membrane (BM) and the overlying tectorial membrane (TM) (*SI Appendix*, Fig. S1*A*). IHCs are the genuine sensory cells that transduce the sound stimuli into electrical signals in the primary auditory neurons. OHCs are mechanical effectors that amplify the sound-evoked movements of the cochlear partition, sharpen its frequency selectivity, and produce waveform distortions (1, 2). A pure-tone stimulus entering the cochlea elicits a traveling wave that propagates along the BM from the cochlear base toward its apex, increasing in amplitude until it peaks at a characteristic place, where the mechanical properties of the cochlea are best tuned to the stimulus frequency. Beyond this characteristic place, the amplitude of the traveling wave declines rapidly to zero (1). The gradual changes in mechanical properties of the cochlea along the BM contribute to establishing the frequency-to-place map such that high-frequency sounds produce maximal responses in the basal region of the cochlea and low-frequency sounds propagate further toward the apex. In the normal cochlea, in response to a pure tone, a locally restricted OHC-driven active process enhances and sharpens the peak of the traveling wave, particularly at low stimulus levels. This causes compressive growth of the wave amplitude at the place tuned to its frequency (1, 2).

Single auditory-neuron tuning curves (TCs) indicate the minimum intensity of a tone required to elicit a neuronal response as a function of tone frequency; they are informative about sound-frequency analysis in the cochlea. These curves display a dip at the characteristic frequency (CF) of the place where

Significance

We show that the submembrane scaffold protein Nherf1 is necessary for correct shaping of outer hair cells stereocilia bundles in the basal cochlea. The mild elevation of hearing thresholds (22–35 dB) of *Nherf1*$^{-/-}$ mice at high frequencies was inconsistent with the loss of outer hair cell functionality in the basal cochlea. Responses of *Nherf1*$^{-/-}$ mice to high-frequency test tones were masked by tones displaying inordinate characteristics in frequency, level, and growth response. We suggest that in *Nherf1*$^{-/-}$ mice, high-frequency vibrations are detected in the unaffected apical cochlea, thus accounting for the powerful masking effect of low-frequency sound. This source of misleading evaluation of high-frequency hearing thresholds and hypervulnerability to low-frequency sound interference should be systematically sought in hearing-impaired patients.

Author contributions: P.A., A.E., and C.P. designed research; K.K., V.M., F.G., B.R., I.F., S.P., I.P., S.L., E.V., and W.X. performed research; U.S. and M.-M.G. contributed new reagents/analytic tools; K.K., V.M., P.A., A.E., and C.P. analyzed data; and P.A., A.E., and C.P. wrote the paper.

The authors declare no conflict of interest.

*This Direct Submission article had a prearranged editor.

Freely available online through the PNAS open access option.

[1]K.K. and V.M. contributed equally to this work.

[2]P.A., A.E., and C.P. contributed equally to this work.

[3]To whom correspondence may be addressed. E-mail: aziz.el-amraoui@pasteur.fr, christine.petit@pasteur.fr, or paul.avan@udamail.fr.

This article contains supporting information online at www.pnas.org/lookup/suppl/doi:10.1073/pnas.1405322111/-/DCSupplemental.

the neuron recorded is connected; this allows the frequency-to-place correspondence to be established. Furthermore, the sharpness of the dip indicates that of the frequency tuning of the innervated IHC (1). Masking TCs, which can be obtained by noninvasive techniques, also provide a reliable evaluation of cochlear frequency selectivity. They depict the minimum intensity of a masking sound required to suppress the response produced by a probe tone near its threshold of detection, as a function of masking sound frequency. The masking TC dip corresponds to the most efficient masking effect and lies near the CF of the cochlear place where the masker and probe sounds interact most efficiently. In the normal cochlea, this CF is close to the probe frequency. The normal masking TCs also present a secondary minimum: a broad, low-frequency segment less sensitive than the dip, called the TC tail. In the tail interval, the low frequency maskers exert their effect at the probe CF place, but only at levels at least 40 dB higher than the intensity that confers masking at the dip frequency.

The most common consequence of OHC impairment is an increased width of TC dips and a decreased dip sensitivity, whereas the sensitivity in the interval of the tail may increase. Frequency shifts of TC dips, less common, are considered to reflect off-frequency hearing (3, 4), a condition reported in patients with dead cochlear zones defined as cochlear intervals in which IHCs and/or associated neurons are nonfunctional. However, intense sound stimulations may be detected in cochlear regions adjacent to dead zones, inferred from the position of where the masking-TC dips have shifted (4). About 60% of deaf people with a hearing threshold above 70 dB have cochlear dead regions (4).

Perturbed frequency selectivity leads to substantial difficulties in understanding speech. Its detection in hearing-impaired individuals is therefore essential and appropriate patient management requires its origin to be determined. This would also help in clarifying the involvement of the various cochlear structures in sound processing and the way they interplay in both normal and pathological conditions. Here, we report a study of the mouse mutant *Nherf1*$^{-/-}$ defective for Na^+-H^+ exchanger regulatory factor 1 (Nherf1), a PDZ domain-containing protein abundant in the OHC hair bundles. Morphological analysis showed hair bundle anomalies of OHCs in the basal, but not apical, region of the cochlea. Electrophysiological investigations revealed an interference, with inordinate characteristics, of low-frequency sounds with the response to high-frequency sounds. The current models of intense low-frequency interference cannot explain these characteristics. We propose an alternative explanation of the extreme vulnerability of *Nherf1*$^{-/-}$ mice to low-frequency sounds.

Results

Nherf1, a PDZ Domain-Containing Protein That Is Abundant in the OHC Hair Bundle. Solute carrier family 9, member 3, regulatory 1 (*Slc9a3r1*) transcripts were identified in a subtracted cDNA library designed to search for proteins preferentially or specifically expressed in sensory epithelia of the inner ear. *Slc9a3r1* encodes Nherf1 (also called Ezrin-radixin-moesin-binding protein of 50 kDa, Ebp50), a member of the Nherf protein family (*SI Appendix*, Fig. S2 *A* and *B*) that consists of four PDZ domain-containing adaptor proteins present in most polarized epithelial cells. In parallel, our work with the yeast two-hybrid system to search for partners interacting with key components of the hair bundle identified Nherf1 as possibly binding to the cytodomain of cadherin-23 (*SI Appendix*, Fig. S2*A*). Cadherin-23 forms both the transient early lateral links that connect stereocilia to each other and to the kinocilium, and the tip link, central to the gating of the mechanoelectrical transduction channels (*SI Appendix*, Fig. S1*B*). Colocalization and coimmunoprecipitation experiments in transfected cells provided further evidence for an interaction between Nherf1 and cadherin-23 (*SI Appendix*, Fig. S2 *C*–*F*).

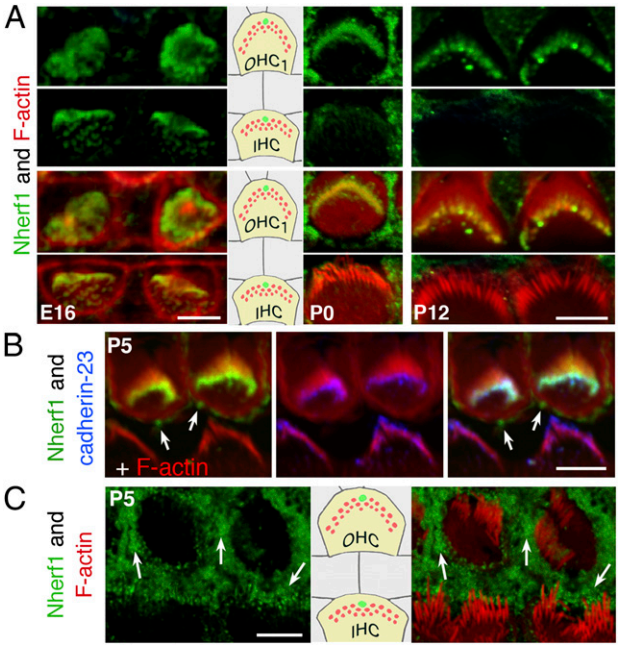

Fig. 1. Nherf1 in the mouse auditory hair cells. (*A*) Nherf1 immunostaining is detected on embryonic day 16 in the stereocilia of IHCs and OHCs. After birth (P0 and P12), Nherf1 was detected only in OHC hair bundles. Nherf1 labeling was intense at the tips of the differentiating stereocilia. (*B* and *C*) Nherf1 and cadherin-23 colocalized at the stereocilia tips. On P5, Nherf1 labeling is weaker in the stereocilia of hair cells, but not in the supporting cells (arrows in *B* and *C*), in *Cdh23*$^{v2j/v2j}$ (*C*) than in control (*B*) mice. (Scale bars, 5 μm.)

The spatiotemporal distribution of Nherf1 in wild-type mice was analyzed using antibodies specific to Nherf1 (Fig. 1 *A*–*C* and *SI Appendix*, Fig. S3*A*). On embryonic day 15.5 (E15.5), Nherf1 was detected in stereocilia as they emerged at the apical surface of the differentiating hair cells in the basal region of the cochlea (*SI Appendix*, Fig. S3*B*). As development proceeded, Nherf1 immunostaining increased in the hair bundles of IHCs and OHCs, with the labeling intensity increasing from the cochlear base to the apex (Fig. 1*A*). By E17, Nherf1 was detected in the hair bundles of all hair cells, throughout the cochlea. The labeling was most intense at the tips of the stereocilia (*SI Appendix*, Fig. S3*C*). At postnatal (P) stages, Nherf1 was no longer detected in IHC hair bundles, whereas the labeling intensity in the OHC hair bundles continued to increase up to P5, and declined from P10 onwards (Fig. 1*A*). Nherf1 and cadherin-23 were both present at the tips of stereocilia in the differentiating OHC hair bundles (Fig. 1*B*), and Nherf1 immunoreactivity was substantially lower in cadherin-23 deficient (*Cdh23*$^{v2j/v2j}$) than control mice (Fig. 1*C*), which is consistent with the two proteins interacting also in vivo.

OHC Hair Bundles from *Nherf1*$^{-/-}$ Mice Display a Base-to-Apex Gradient of Abnormal Shapes. Scanning electron microscopy analysis of the differentiating and mature cochlea in *Nherf1*$^{-/-}$ mice showed major hair bundle anomalies in OHCs, but not in IHCs (Fig. 2). At early (P0–P5) and later (P20–P60) postnatal stages, the OHC hair bundles had rounded, hooked, wavy, or linear shapes (Fig. 2 *A* and *B* and *SI Appendix*, Fig. S4 *A* and *B*). However, the length, and the number of stereocilia per OHC hair bundle, the regular staircase-like pattern of the stereocilia rows, and the hair-bundle links that connect the growing stereocilia, did not differ between *Nherf1*$^{-/-}$ and control mice (Fig. 2). Despite the persistence of the links between the kinocilium and adjacent stereocilia, the positioning of the kinocilia relative to their expected positions along the planar cell polarity axis (Fig. 2*D*) was abnormal

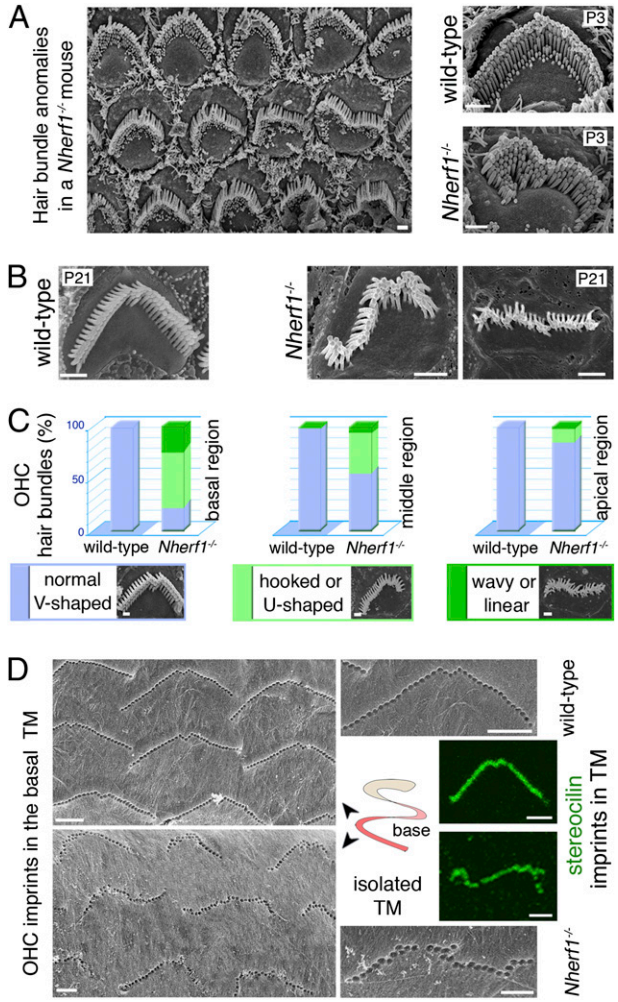

Fig. 2. Abnormal OHC hair bundle shapes in *Nherf1*$^{-/-}$ mice. (*A* and *B*) In *Nherf1*$^{-/-}$ mice, the shapes of the OHC hair bundles are abnormal mainly in the basal cochlear region: wavy, linear, and hooked shapes are observed. (*C*) Abnormally shaped OHC hair bundles (light and dark greens, *Lower*) and normal, V-shaped hair bundles (blue) were counted in each cochlear region (basal, middle, apical) in *Nherf1*$^{-/-}$ and wild-type mice: in *Nherf1*$^{-/-}$ mice, 80 ± 5% of OHCs in the cochlear basal region displayed abnormal hair bundle shapes. (*D*) In *Nherf1*$^{-/-}$ mice (*Lower*), OHC imprints on the TM at the cochlear base (also labeled by anti-stereocilin antibodies, green) predominantly correspond to misshaped arrays of OHC stereocilia. (Scale bars, 1 μm.)

in OHCs at the cochlear base in P3–P7 *Nherf1*$^{-/-}$ mice (*SI Appendix*, Fig. S4*C*: only 26 ± 2% of the kinocilia at the cochlear base were present within 6° of the planar polarity axis, versus 58 ± 3% for wild-type mice). Quantitative analysis of the *Nherf1*$^{-/-}$ cochlea at P20–P25 revealed a conspicuous cochlear base–apex gradient of hair bundle shape anomalies: 80 ± 5%, 50 ± 5%, and 10 ± 2% of hair bundles were abnormal in the basal, middle, and apical regions of the cochlea, respectively. These anomalies were very pronounced at the base, and subtler at the apex of the cochlea (Fig. 2*C* and *SI Appendix*, Fig. S5 *A*–*C*).

In wild-type mice, the tallest stereocilia of the OHC hair bundles are anchored in the TM, where they form characteristic V-shaped imprints at its lower aspect (Fig. 2*D*). These imprints provide a well-defined overall view of the shape of the OHC hair bundle's anchor in the TM. In *Nherf1*$^{-/-}$ mice, these imprints were present, but they were severely misshaped for 90 ± 5% of OHCs at the cochlear base and only affected, and less strongly so, for 15 ± 3% of OHCs at the apex (Fig. 2*D* and *SI Appendix*, Fig. S5*D*). Antibodies directed against stereocilin, a protein present at the interface between the tips of the tallest stereocilia of the OHCs and the TM, labeled the stereocilia imprints in the TM (Fig. 2*D* and *SI Appendix*, Fig. S5*E*). This confirms that the anchoring of these stereocilia in the TM was normal, despite the abnormal shapes of the hair bundles.

In *Nherf1*$^{-/-}$ Mice, Mild Midhigh Frequency Threshold Elevation Contrasts with Severely Defective Responses of the OHCs at the Cochlear Base. We next analyzed the hearing sensitivity of *Nherf1*$^{-/-}$ mice at P21–P25 by measuring the thresholds of distortion-product otoacoustic emissions (DPOAEs) and auditory brainstem responses (ABRs) to brief pure-tone stimuli in the 5- to 40-kHz frequency

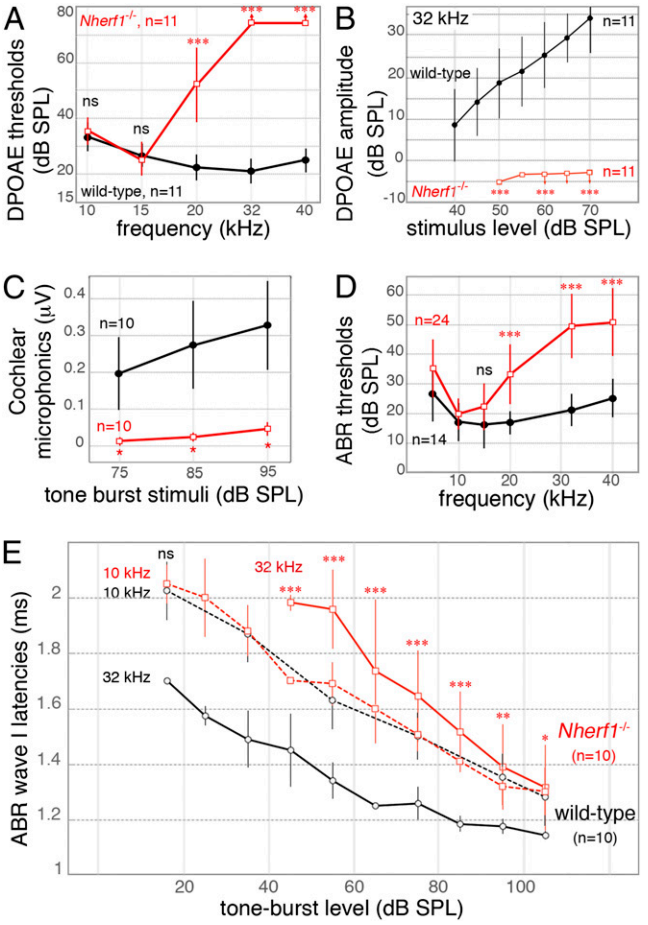

Fig. 3. Hearing impairment at midhigh sound frequencies in *Nherf1*$^{-/-}$ mice. (*A*–*D*) DPOAEs, CM potentials, and ABRs in P20–P25 wild-type (black) and *Nherf1*$^{-/-}$ (red) mice. (*A*) DPOAE thresholds (±SD) at and above 20 kHz are significantly higher in *Nherf1*$^{-/-}$ mice than in wild-type mice. (*B*) The DPOAEs (±SD) at 32 kHz are indistinguishable from noise background in *Nherf1*$^{-/-}$ mice (red, downward-pointing arrows; $n = 11$). In these cases, DPOAE thresholds were arbitrarily set at 75 dB SPL, the highest intensity stimulus tested. (*C*) The amplitude of the CM potential for a 10-kHz tone-burst stimulus (±SEM), measured at the round window, was significantly smaller in *Nherf1*$^{-/-}$ mice ($n = 10$) than in control mice ($n = 10$). (*D*) Beyond 15 kHz, the ABR thresholds (±SD) were significantly higher in *Nherf1*$^{-/-}$ mice than in control littermates. (*E*) ABR wave-I timing at 10 and 32 kHz as a function of stimulus sound level in *Nherf1*$^{-/-}$ mice. For 10-kHz tone-burst sound stimuli, average ABR wave-I latencies (±SD) did not differ between wild-type (black dashed line) and *Nherf1*$^{-/-}$ mice (red dashed line), regardless of the strength of the stimulus. The latency of the 32-kHz ABR wave I for *Nherf1*$^{-/-}$ mice (red plain line) was shifted upward by 0.4–0.6 ms relative to that for wild-type mice (black plain line) between 45 and 85 dB SPL. *P < 0.05, **P < 0.01, and ***P < 0.001. ns, not significant.

NEUROSCIENCE

range (Fig. 3). There was no significant difference in DPOAE thresholds between *Nherf1*$^{-/-}$ ($n = 11$) and wild-type ($n = 11$) mice for primary tone frequencies in the 5- to 15-kHz range ($P > 0.99$; Fig. 3*A*). By contrast, between 19 and 28 kHz, DPOAE thresholds in *Nherf1*$^{-/-}$ mice were higher than normal and approached the upper limit of detectability (Fig. 3*A* and *SI Appendix*, Fig. S6*A*), and DPOAEs were undetectable at 32 kHz in all mutant mice (Fig. 3*B*). The corresponding DPOAE threshold elevations were 29.7 ± 14 dB at 20 kHz and >47.5 dB at 32 kHz ($P < 0.0001$; Fig. 3*A*). We also measured the cochlear microphonic potential (CM), which, being proportional to the sound-induced transducer potentials of the OHCs of the basal-most cochlear region, is an indicator of their mechanoelectrical transduction (5): the mean CM was 10 times smaller in *Nherf1*$^{-/-}$ mice ($n = 10$) than in wild-type mice ($n = 10$) ($P < 0.05$, Fig. 3*C*), indicating a drastic decrease of OHC function in the cochlear base. The ABR thresholds of *Nherf1*$^{-/-}$ mice ($n = 24$) were within the normal range for tone-burst frequencies below 15 kHz ($P = 0.2307$ at 15 kHz), consistent with the normal DPOAEs in the low-frequency interval. Above 15 kHz, ABR thresholds were only moderately higher than in control mice (by 22.2 ± 10 dB at 20 kHz and 35 ± 12 dB between 32 and 40 kHz, $P < 0.0001$) (Fig. 3*D*), at odds with the DPOAE defects.

We analyzed the latencies of the first peak of the compound action potential (CAP) and its ABR wave-I correlate, which reflect the synchronous response of the auditory nerve to tone bursts. They depend on the propagation delay of the wave associated with the stimulus to the responding cochlear site. They also include intensity-dependent contributions from the local processing mechanisms in the sensory cells. In wild-type mice, CAP latencies in response to a 10-kHz probe were between 2.02 ms at the ABR threshold and 1.28 ms at 105 dB sound-pressure level (SPL); at 32 kHz, the range was from 1.70 ms at the ABR threshold to 1.15 ms at 105 dB SPL ($n = 10$) (Fig. 3*E*). The difference in CAP latencies at a given sound level between 10 kHz and 32 kHz was consistent with the base-to-apex cochlea frequency map. In *Nherf1*$^{-/-}$ mice ($n = 10$), the CAP latency plot at 10 kHz was similar to that for control mice ($P > 0.85$, Fig. 3*E*): at 32 kHz, the CAP latency was between 1.97 and 1.31 ms, and thus in the same range as for 10 kHz tone bursts (Fig. 3*E*). Even at stimulus levels of 95 ($P < 0.01$) and 105 ($P < 0.05$) dB SPL, such that OHC function negligibly influences the timing and size of cochlear responses, CAP latency at 32 kHz remained at least 0.18 ms longer in *Nherf1*$^{-/-}$ than in control ears (Fig. 3*E* and *SI Appendix*, Fig. S6*B*).

Masking Tuning Curves for Midhigh Frequency Sounds Display Major Shifts Toward Low Frequencies in *Nherf1*$^{-/-}$ Mice. To examine further the functional status of basal OHCs in *Nherf1*$^{-/-}$ mice, masking TCs were used to measure their frequency selectivity (Fig. 4). Masking TCs show how the relative frequency distance between masker and probe frequencies shapes their interaction at the cochlear site where this interaction, and thus the masking effect, occurs. Probe frequencies were set either at 10 kHz, a frequency with normal ABR hearing thresholds (Fig. 3 *A* and *D*), or between 20 and 40 kHz, corresponding to frequencies at which cochlear responses were clearly affected in all *Nherf1*$^{-/-}$ mice (Fig. 3 *A* and *D*). In the normal cochlea, the masking-TC dip lies close to the frequency of the probe tone, irrespective of the tested probe frequency (10, 27, 32, or 40 kHz; Fig. 4*A*). In *Nherf1*$^{-/-}$ mice at 10 kHz ($n = 12$), masking TCs displayed a narrow dip near the probe frequency and a broad low-frequency tail, almost superimposed on those in *Nherf1*$^{+/+}$ ($n = 12$) mice (Fig. 4*A*). By contrast, for probe frequencies equal to or above 20 kHz ($n = 33$), the masking TCs in *Nherf1*$^{-/-}$ mice were markedly abnormal: there were few dip-like minima around the probe frequency and only for masker intensities exceeding 100 dB SPL (Fig. 4 *A* and *B* and *SI Appendix*, Fig. S7*A*, *Right*). Conversely, intense masking was systematically observed for masker tones of lower frequencies, with a mean of 12.7 ± 5.3 kHz,

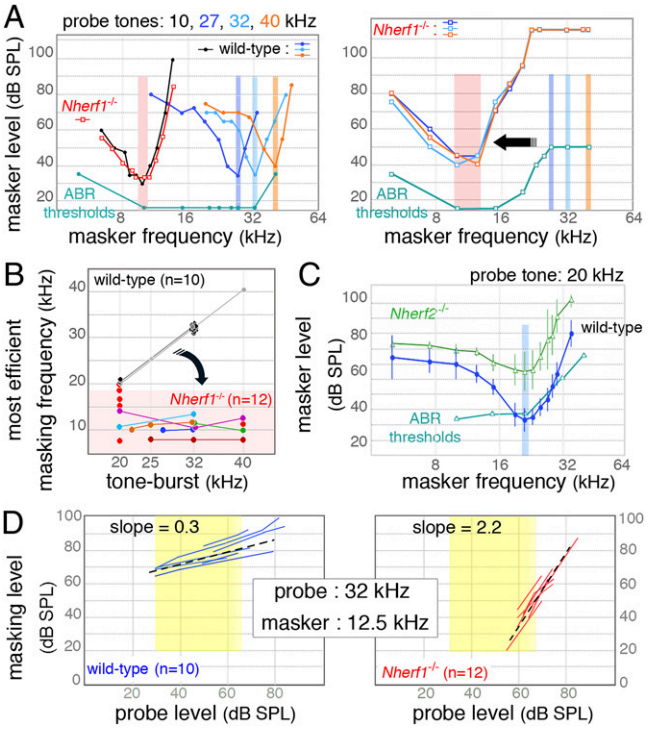

Fig. 4. Abnormally efficient masking of midhigh frequency sounds by lower frequency sounds in *Nherf1*$^{-/-}$ mice. (*A*) For a low-frequency probe tone (10 kHz) (*Left* graphs on the *Left*), the masking TC recorded in a *Nherf1*$^{-/-}$ mouse did not differ from that in a wild-type mouse. The most efficient masker (dip of the V-shaped curve) was at or near the probe frequency and within 10 dB of the probe intensity (see ABR thresholds curve). For midhigh frequency probe tones [27 (blue), 32 (green), and 40 (orange) kHz], the efficient masking (the dip of the TC) was shifted toward low-frequency sounds (light red background), on average at 12.5 kHz in the *Nherf1*$^{-/-}$ mice. (*B*) Scatterplots of the most efficient masking frequency (TC dip frequency) as a function of probe frequency in wild-type (gray to black dots) and *Nherf1*$^{-/-}$ (colored dots) mice. Colored lines connect data points collected in the same ear at the different probe frequencies as indicated. In *Nherf1*$^{-/-}$ mice ($n = 12$), the efficient masking for midhigh frequency sounds (beyond 20 kHz) was shifted toward low-frequency sounds. (*C*) For a 20-kHz probe tone in *Nherf2*$^{-/-}$ mice, the most efficient masking (still centered near the probe frequency) was at higher levels than for wild-type mice. (*D*) Growth of masker (GOM) curves for off-frequency conditions (signal at 32 kHz and masker at 12.5 kHz). In the intermediate range of probe tone-burst intensities (yellow zone), the slope of the GOM curves for wild-type mice was shallow (0.35 dB/dB, $n = 10$) and that for *Nherf1*$^{-/-}$ mice was much steeper (2.2 dB/dB, $n = 12$). The large GOM allowed compression measurements to be made with probe tone-burst levels not exceeding 65 dB SPL (yellow zone), which kept the risk of spectral splatter under control.

such that the most efficient masker was 2.15 octaves below the probe with the highest frequency tested (40 kHz).

Our calibration of the acoustic setup, and the masking TCs obtained in *Nherf2*$^{-/-}$ mice (Fig. 4*C* and *SI Appendix*, Figs. S8 *C* and *D* and S9), defective for another member of the Nherf protein family, rule out any possibility of participation of the spectral splatter to the shift of masking toward low-frequency sounds. The low-frequency minimum of masking TCs in *Nherf1*$^{-/-}$ mice peaked for masker levels a mean of 15 ± 11 dB lower than the probe tone, in some cases 25 dB lower (Fig. 4 *A* and *B*). In each mutant, the frequency interval of this efficient masking was within the frequency range of its normal ABR and DPOAE thresholds (red background in Fig. 4 *A* and *B*). For any single ear, masking TCs with probes of different frequencies between 20 and 40 kHz, such that DPOAE thresholds at these frequencies exceeded 70 dB ($n = 7$), systematically coincided within 5 dB

of each other over the whole frequency range of tested maskers (Fig. 4*B* and *SI Appendix*, Fig. S7*A*).

In normal healthy ears, maximum masking occurs when the frequency of at least one of the two interfering sounds, the probe or the masker, coincides with the CF of the cochlear place where the masking effect is generated (2, 4, 6). In an active cochlea, the BM vibration for intermediate stimulus intensities (20–80 dB SPL) undergoes compressive amplification of its displacements solely at the CF place of the stimulus, where it increases by only about 0.3 dB/dB increase of sound level in the ear canal. By contrast, cochlear vibrations at places distant from the CF place, not influenced by OHC activity, increase linearly by 1 dB/dB (1). Which of the two sounds is at CF at the interference place can be determined by measuring the increase of the efficient masker intensity with increasing probe intensity (growth of masker, GOM) (6).

In wild-type mice, when probe and masker frequencies were close to each other (20 and 19 kHz, or 32 and 30 kHz, respectively), a paradigm referred to as "on-frequency" masking, the GOM was about 1 dB/dB: both the probe and masker cochlear responses displayed similar compressed rates of increase at their interference place (20 kHz or 32 kHz CF place, respectively) (6). In *Nherf1*$^{-/-}$ mice with normal ABRs at 10 kHz, a frequency at which on-frequency masking was efficient, the GOM was also about 1 dB/dB (Fig. 4*D* and *SI Appendix*, Fig. S7*B*).

We then examined masking when probe and masker are set at very different frequencies, e.g., 32 and 12.5 kHz, respectively, referred to as "off-frequency" masking. In *Nherf1*$^{+/+}$ mice, the GOM was 0.35 dB/dB ($n = 10$) for probe intensities between 30 and 65 dB SPL (Fig. 4*D*), and was slightly steeper above 65 dB SPL. This is coherent with the reported decrease in compression at increasing levels (1). In *Nherf1*$^{-/-}$ mice ($n = 12$), the pattern of masker growth under the same stimulation conditions was reversed: the GOM was 2.2 dB/dB for probe intensities in the 50- to 65-dB SPL range (Fig. 4*D*). This inversed pattern indicates that the efficient low-frequency maskers undergo more compression than the probe sound that they mask, suggesting that maskers act near their own CF place. This raises questions about the idea that in the 50- to 65-dB SPL range (Fig. 4*D*), the place where the high-frequency probe stimulus elicits its CAP has a high CF (*SI Appendix*, Table S1).

Discussion

The hearing impairment in *Nherf1*$^{-/-}$ mice is characterized by a transition between near-normal low-frequency responses, below 15 kHz, and abnormal high-frequency responses above 15 kHz (Fig. 3 *A* and *C*). Consistent with this, anomalies of OHC hair bundles are rare at the cochlear apex, more prevalent in the middle region of the cochlea, and involve 95% of OHCs at the cochlear base. The lack of Nherf1-mediated structural and signaling activities in these mutant mice probably results in slackening of stereocilia membrane tension, as suggested by the irregular shapes of OHC hair bundles. During hair bundle differentiation, cell intercalations and cell–cell junction remodeling concomitant with the convergent extension process are conspicuous at the cochlear base but are rare at the apex. This may explain the gradient of the prevalence of anomalies increasing from apex to base. The absence of high-frequency DPOAEs and the about 10-fold reduction of CM potential amplitude in *Nherf1*$^{-/-}$ mice indicate an overall lack of activity of the basal OHCs. This is not consistent with the small magnitude of ABR threshold elevations above 20 kHz. The OHCs are believed to influence the sensitivity of the cochlear response by acting in a feedback loop, which amplifies cochlear vibrations by up to 60 dB, when cycle-by-cycle OHC feedback occurs with the appropriate timing. Accordingly, a 60-dB increase in ABR thresholds in the high-frequency range was expected in *Nherf1*$^{-/-}$ mice (1), such that the increase of 22–35 dB that was observed was surprising (Fig. 3).

The apparent mildness of ABR threshold shifts in *Nherf1*$^{-/-}$ mice is also inconsistent with the substantial abnormality of their frequency selectivity. Modified masking TCs, such that maximally efficient masking frequencies are below the probe frequency, have already been reported in two conditions: the so-called "hypersensitivity of the tail" (7) and "off-frequency detection" (4).

In the hypersensitivity of the tail cases, TCs of individual auditory neurons innervating IHCs at cochlear places where OHCs stereocilia or these cells themselves are absent, have no sensitive dip at CF and display abnormally great sensitivity in response to low frequencies (7). This hypersensitivity is attributed to increased shear motion of the TM, due to slackened coupling to the organ of Corti in the absence of functional OHC; this is believed to confer on the basal cochlea an increased sensitivity to low-frequency vibrations (7). Comparison of abnormal neuronal TCs and normal reference TCs at similar CFs show that low-frequency responses emerge in such situations at levels 10–15 dB lower than normal (7–9). In the less severe condition in which OHCs are damaged yet still present, the dips of neuronal TCs are found near the normal CF, and low-frequency tails with increased sensitivity are usually observed, the tail minimum being at about the same level as the dip. However, several of our experimental findings in *Nherf1*$^{-/-}$ mice are not consistent with this model. First, the masking of high-frequency probes by low-frequency maskers in *Nherf1*$^{-/-}$ mice is much stronger than reported for cases ascribed to hypersensitivity of the tail (7). Low-frequency maskers at levels 15 dB and sometimes 25 dB below the probe level on average exerted effective masking in *Nherf1*$^{-/-}$ mice, whereas tail levels for low-frequency interference in cases of hearing loss of other types are between 15 and 25 dB higher than the probe level (Fig. 4*C* and *SI Appendix*, Fig. S8*D*); in cases of hypersensitivity of the tail as described elsewhere, masking would not occur at levels lower than probe level. Second, the frequency interval at which a hypersensitive tail is found should relate directly to the mechanical coupling of the TM to OHCs at the probe–CF place, where CAP responses to the probe are elicited. This is not the case in *Nherf1*$^{-/-}$ mice, in which probe frequencies could vary from 20 to 40 kHz with no influence on masking TC shapes or dip positions. Indeed, the masking TC shapes in a given ear seemed to be related to the low-frequency interval of normal auditory sensitivity in that ear. Third, according to the hypersensitivity of the tail hypothesis, low frequencies exert their masking effect at the CF place of the high-frequency probe. Whether OHCs are functional or not, it is generally believed that vibrations, far from their own CF place, can undergo neither amplification nor compression (1), and therefore the expected GOM should be lower than 1 dB/dB. It does not appear possible to reconcile the observed GOM in *Nherf1*$^{-/-}$ mice with this interpretative model. Finally, unlike in the case of the hypersensitivity of the tail (7), *Nherf1*$^{-/-}$ OHC hair bundles are still anchored in the TM.

The other hypothesis, off-frequency detection, mirrors the hypersensitivity of the tail model by positing that high-frequency probes near their ABR threshold (at levels <65 dB SPL) are not detected at the place tuned to the probe itself but at the CF places of best maskers, i.e., within the normally sensitive and immediately apical cochlear region. In the typical case of a dead basal cochlear region, high-frequency probes are indeed detected at sensitive places not tuned to those probes but adjacent to the dead cochlear region (4). In *Nherf1*$^{-/-}$ mice, the GOM data in off-frequency settings show a 2.2 dB/dB slope, which indicates that the maskers, but not the probes, undergo compression; this implies that the places where masking occurs also actively process masker-induced vibrations (1) (*SI Appendix*, Table S1). The unusual ability of low-frequency maskers to act at levels up to 25 dB lower than the detection threshold of the high-frequency probe provides further support to the notion that the probe is detected at places where the masker is amplified. In the case of dead cochlear regions, sensitive places just apical to a dead zone can still be reached by the traveling BM wave, but the probe intensity would usually have to exceed 70 dB SPL to overcome the strong apical-ward attenuation beyond the CF place (70 dB/octave) (10). In *Nherf1*$^{-/-}$ mice, the masking TC dips could shift

downward by up to two octaves with neural responses to 32 or 40 kHz probe tone bursts at 60 dB SPL being masked optimally by masker tones at 10–12 kHz (Fig. 4*A*), thus raising the critical issue of how high-frequency vibrations could have reached the apical detection site as they could not have traveled along the BM. A mechanism of apical propagation other than Békésy's BM traveling wave is presumably therefore operating in *Nherf1*$^{-/-}$ mice. This mechanism differs by its ability to spread medium-level high-frequency vibrations toward the cochlear apical region. Various modes of vibration have been detected in the cochlea, and they include a fast acoustic-pressure wave traveling in cochlear duct fluids (11), but which has little effect on hair bundle deflection. The latencies of the high-frequency ABRs of *Nherf1*$^{-/-}$ mice, if produced off frequency by an acoustic-pressure wave, should be as short as in *Nherf1*$^{+/+}$ mice. The Reissner membrane has recently been described to support the propagation of vibrations that contribute significantly to the excitation of the apical-most part of the cochlea (12). Recent ex vivo investigations of the viscoelastic properties of the TM suggest that it is possible for a wave to travel longitudinally along this membrane (13–15). If the in vivo properties are similar to those reported ex vivo, the features of the TM wave might allow it to propagate high-frequency vibrations to the apex of *Nherf1*$^{-/-}$ cochleas. IHC excitation requires the deflection of stereocilia bundles, and TM vibrations may cause such deflection even when the BM and reticular lamina do not vibrate.

How can high-frequency waves propagate along the TM from basal places? *Nherf1*$^{-/-}$ mice have normal numbers of OHCs in the basal region that, strikingly, display persistent mechanical coupling to the TM (Fig. 2). Consequently, passive vibrations of the basal BM might be transmitted to the TM. Normally, vibrations of the reticular lamina differ in amplitude and timing from those of the BM and both display rapid phase changes in the longitudinal direction near the CF, due to OHC mechanical feedback (16); this likely hampers the efficacy of any leak to the TM in wild-type conditions. In *Nherf1*$^{-/-}$ mice with defective basal OHCs, one would expect BM motion, although weak, to occur in phase with the reticular lamina over a broad region, which may act as a beamforming mechanism resulting in significant TM motion. It is also possible that the disrupted stiffness gradient of OHC stereocilia bundles in *Nherf1*$^{-/-}$ mice favors this beamforming mechanism, whereas in the normal case, the stiffness gradient would oppose it by controlling the spatial decay of waves in the basoapical direction. Ex vivo, TM waves undergo little attenuation over hundreds of micrometers and travel at 3–6 m/s, in a smooth frequency- and place-dependent manner (13). This would translate into an ∼0.4-ms travel time between the places with CFs at 40 and 10 kHz, which is consistent with the observed shift in wave-I latencies of ABRs to high-frequency tone bursts in *Nherf1*$^{-/-}$ mice (Fig. 3*E*). The off-frequency detection model would also account for the need for on-frequency maskers to be about 40 dB more intense than the 20 and 32 kHz probes, because the interaction between these probes and maskers is assumed to occur apically at places tuned to the best maskers, and which respond nonlinearly only to sounds near their CF. Contrary to the normal cases in which masking has a strong suppressive component, in *Nherf1*$^{-/-}$ mice, the only possible masking mechanism would be the line-busy mechanism by which the masker saturates the neuronal activity and swamps the transient probe-induced activity (17); this requires the masker to be about 40 dB more intense than the probe.

In summary, the off-frequency detection mechanism can account for the results we report in *Nherf1*$^{-/-}$ mice without any need for altering the basic tenets of cochlear mechanics. We propose that a mode of propagation along the TM that has been described in vitro may extend abnormally in the apical direction via the persisting coupling between inactive OHCs and the TM. In patients with a similar abnormality, this would bias the interpretation of audiometric evaluation by suggesting a misleadingly mild high-frequency hearing impairment. This would in turn affect the hearing-aid fitting procedure. The detection of medium-level high-frequency sounds despite a severely damaged cochlear base may provide a beneficial natural frequency transposition, akin to that implemented by hearing aids that numerically displace inaudible high-frequency components to a midfrequency interval to which the ear remains more sensitive. However, our findings in *Nherf1*$^{-/-}$ mice suggest that transposed information is so vulnerable to interference from low-frequency sounds that patients are likely to have major difficulties hearing in noisy environments, inconsistent with a hearing impairment misdiagnosed as "mild." Therefore, screening for this newly identified type of cochlear dysfunction is essential for appropriate clinical evaluations of patients with hearing disorders. Our study indicates that this problem could be identified by systematic screening for inconsistency between ABR and DPOAE measurements, and that abnormal psychophysical masking test results would reveal the unusual detrimental impact of low-frequency sounds.

Materials and Methods

A detailed description of the methods is available in *SI Appendix, Materials and Methods*. *Nherf1*$^{-/-}$, *Nherf2*$^{-/-}$, and *Cdh23*$^{v2j/v2j}$ mice were used. Immunofluorescence analysis, study of the structure of the auditory hair cells by light and scanning electron microscopy, and the in vivo measurements for physiological analysis were performed. Experiments with animals were carried out using protocols approved by the Animal Use Committee of INSERM and Institut Pasteur.

ACKNOWLEDGMENTS. We thank J.-P. Hardelin and J. Boutet de Monvel for their suggestions on the manuscript and S. Delmaghani, D. Weil, and M. Muraki for their assistance. This work was supported by the Japan Society for the Promotion of Science and Uehara Memorial Foundation (K.K.), European Research Council (ERC)-Hair Bundle (ERC-2011-ADG_20110310), LABEX Lifesenses (ANR-10-LABX-65), Réunica-Prévoyance, Novalis Taitbout, BNP-Paribas, and Fondation Voir et Entendre (C.P.).

1. Robles L, Ruggero MA (2001) Mechanics of the mammalian cochlea. *Physiol Rev* 81(3): 1305–1352.
2. Avan P, Büki B, Petit C (2013) Auditory distortions: Origins and functions. *Physiol Rev* 93(4):1563–1619.
3. O'Loughlin BJ, Moore BC (1981) Off-frequency listening: Effects on psychoacoustical tuning curves obtained in simultaneous and forward masking. *J Acoust Soc Am* 69(4):1119–1125.
4. Moore BC, Alcántara JI (2001) The use of psychophysical tuning curves to explore dead regions in the cochlea. *Ear Hear* 22(4):268–278.
5. He W, Porsov E, Kemp D, Nuttall AL, Ren T (2012) The group delay and suppression pattern of the cochlear microphonic potential recorded at the round window. *PLoS ONE* 7(3):e34356.
6. Plack CJ, Oxenham AJ (1998) Basilar-membrane nonlinearity and the growth of forward masking. *J Acoust Soc Am* 103(3):1598–1608.
7. Liberman MC, Dodds LW (1984) Single-neuron labeling and chronic cochlear pathology. III. Stereocilia damage and alterations of threshold tuning curves. *Hear Res* 16(1):55–74.
8. Dallos P, Harris D (1978) Properties of auditory nerve responses in absence of outer hair cells. *J Neurophysiol* 41(2):365–383.
9. Versnel H, Prijs VF, Schoonhoven R (1997) Auditory-nerve fiber responses to clicks in guinea pigs with a damaged cochlea. *J Acoust Soc Am* 101(2):993–1009.
10. Richter CP, Evans BN, Edge R, Dallos P (1998) Basilar membrane vibration in the gerbil hemicochlea. *J Neurophysiol* 79(5):2255–2264.
11. He W, Fridberger A, Porsov E, Grosh K, Ren T (2008) Reverse wave propagation in the cochlea. *Proc Natl Acad Sci USA* 105(7):2729–2733.
12. Reichenbach T, Stefanovic A, Nin F, Hudspeth AJ (2012) Waves on Reissner's membrane: A mechanism for the propagation of otoacoustic emissions from the cochlea. *Cell Reports* 1(4):374–384.
13. Ghaffari R, Aranyosi AJ, Freeman DM (2007) Longitudinally propagating traveling waves of the mammalian tectorial membrane. *Proc Natl Acad Sci USA* 104(42): 16510–16515.
14. Ghaffari R, Aranyosi AJ, Richardson GP, Freeman DM (2010) Tectorial membrane travelling waves underlie abnormal hearing in Tectb mutant mice. *Nat Commun* 1:96.
15. Lamb JS, Chadwick RS (2011) Dual traveling waves in an inner ear model with two degrees of freedom. *Phys Rev Lett* 107(8):088101.
16. Chen F, et al. (2011) A differentially amplified motion in the ear for near-threshold sound detection. *Nat Neurosci* 14(6):770–774.
17. Delgutte B (1996) Physiological models for basic auditory percepts. *Auditory Computation*, eds Hawkins HH, McMullen TA, Popper AN, Fay RR (Springer, New York), pp 157–220.